J. Fluid Mech. (2002), *vol.* 463, *pp.* 361–375.
DOI: 10.1017/S0022112002001040 Printed in the United Kingdom

Hydromagnetic Taylor–Couette flow: numerical formulation and comparison with experiment

By A. P. WILLIS AND C. F. BARENGHI

Department of Mathematics, University of Newcastle, Newcastle NE1 7RU, UK

(Received 16 July 2001 and in revised form 21 February 2002)

Taylor–Couette flow in the presence of a magnetic field is a problem belonging to classical hydromagnetics and deserves to be more widely studied than it has been to date. In the nonlinear regime the literature is scarce. We develop a formulation suitable for solution of the full three-dimensional nonlinear hydromagnetic equations in cylindrical geometry, which is motived by the formulation for the magnetic field. It is suitable for study at finite Prandtl numbers and in the small Prandtl number limit, relevant to laboratory liquid metals. The method is used to determine the onset of axisymmetric Taylor vortices, and finite-amplitude solutions. Our results compare well with existing linear and nonlinear hydrodynamic calculations and with hydromagnetic experiments.

1. Introduction

The motion of an incompressible viscous fluid between concentric rotating cylinders is one of the most important problems of fluid dynamics and is much studied as a benchmark to investigate issue of instability and nonlinear behaviour. Taylor (1923) found that if the rotation of the inner cylinder is greater than some critical value then circular-Couette flow (CCF) becomes unstable to axisymmetric perturbations. A secondary flow appears which has axial and radial motion in the form of pairs of toroidal vortices, now known as the Taylor-vortex flow (TVF). If the inner cylinder is driven faster then this flow becomes unstable to non-axisymmetric perturbations. Azimuthal waves appear in the Taylor vortices and the whole pattern rotates at some wave speed (wavy modes).

In his landmark 1961 book on stability theory, Chandrasekhar devoted equal attention to the hydrodynamic and the hydromagnetic Couette problems; the latter is the case in which the fluid is a conducting liquid (e.g. mercury, liquid gallium, liquid sodium) and a magnetic field is applied externally. Despite this early interest in the hydromagnetic Couette problem, which included experiments performed by Donnelly & Ozima (1962) and by Donnelly & Caldwell (1963), most of the activity of the following years was devoted to the hydrodynamic case. Among the few studies of the effects of the magnetic field it is worth recalling the works by Velikhov (1959), Kurzweg (1963), Roberts (1964), who extended Chandrasekhar's theory to non-axisymmetric bifurcations from circular-Couette flow, Chang & Sartory (1967) and Baylis & Hunt (1971) at finite aspect ratio. Later Tabeling (1981), using a method similar to Davey's (1962) amplitude expansion, calculated the effective viscosity of axisymmetric flow in the Taylor-vortex flow regime; he compared with Donnelly's (1962) experiments which indicate that the onset of wavy vortices is significantly inhibited by the magnetic

field. Nagata (1996) has more recently investigated nonlinear solutions in the planar geometry, and Hollerbach (2000*a*) shows Taylor cells in spherical geometry.

The aim of this paper is to investigate effects induced on Couette flow by an externally applied magnetic field. This paper is meant to be the first of a series and is dedicated to the development of a suitable formulation for solving numerically the governing nonlinear three-dimensional magnetohydrodynamic (MHD) equations in the cylindrical Couette geometry. The numerical method which we propose can be used for any value of radius ratio, is suitable for time stepping, has good stability features, is relatively easy to program and is more accurate than existing methods.

Our work is also motivated by the renewed interest in MHD flows in confined geometries which arises from current and planned experiments to produce dynamo action in the laboratory (Gailitis *et al.* 2001; Stieglitz & Muller 2001). It must be stressed that our work does not apply directly to the dynamo problem for two reasons. First, the cylindrical Couette configuration is a possible geometry for these studies, but it has not been used in experiments yet, and it may prove to be not the most efficient one (Laure, Chossat & Daviaud 2000). Secondly, our investigation refers primarily to bifurcations at relatively small Reynolds numbers, while the dynamo experiments require rather large Reynolds numbers due to the small magnetic Prandtl number of liquid metals. Despite these two limitations, our work is related to the dynamo problem because it is important to have precise results for small Reynolds number MHD flows in order to develop and test modern acoustic flow visualization techniques, Kikura, Takeda & Durst (1999), which offer the best chance to detect flow patterns in MHD dynamos. The lack of flow visualization has clearly held back progress in the hydromagnetic Couette problem compared to the hydrodynamic case.

2. Equations

The equations governing incompressible hydromagnetic flow are

$$\partial_t \boldsymbol{u} + (\boldsymbol{u}\cdot\nabla)\boldsymbol{u} = -\frac{1}{\rho}\nabla p + \nu\nabla^2\boldsymbol{u} + \frac{1}{\rho\mu_0}(\nabla\wedge\boldsymbol{B})\wedge\boldsymbol{B}, \quad \nabla\cdot\boldsymbol{u} = 0, \tag{2.1a,b}$$

$$\partial_t \boldsymbol{B} = \lambda\nabla^2\boldsymbol{B} + \nabla\wedge(\boldsymbol{u}\wedge\boldsymbol{B}), \quad \nabla\cdot\boldsymbol{B} = 0, \tag{2.1c,d}$$

where $\boldsymbol{u}$ is the fluid's velocity, $\boldsymbol{B}$ the magnetic field, p the pressure, ρ the density, ν the kinematic viscosity, λ the magnetic diffusivity and μ_0 the magnetic permeability. Hereafter we assume that ρ, ν, λ and μ_0 are constant. The fluid is contained between two concentric cylinders of inner radius R_1 and outer radius R_2. The inner and outer cylinders rotate at constant angular velocities Ω_1 and Ω_2 respectively. A magnetic field $\boldsymbol{B}_0 = \mu_0 H\hat{\boldsymbol{z}}$ is applied externally in the axial direction. We make the usual simplifying assumption that the cylinders have infinite length and use cylindrical coordinates (r,θ,z).

Throughout the rest of this work we will make the variables dimensionless using the following scales:

$\delta = R_2 - R_1$ length (gap width); $\quad \delta^2/\nu$ time (viscous diffusion);

ν/δ velocity; $\quad \mu_0 H$ magnetic field.

We introduce the following dimensionless parameters: radius ratio (η), Reynolds numbers (Re_1 and Re_2), Hartmann number (Q) and magnetic Prandtl number (ξ)

defined as

$$\eta = R_1/R_2; \quad Re_i = \frac{R_i \Omega_i \delta}{\nu}, \quad i = 1, 2; \quad Q = \frac{\mu_0^2 H^2 \sigma \delta^2}{\rho \nu}; \quad \xi = \frac{\nu}{\lambda}. \tag{2.2}$$

The dimensionless forms of (2.1*a*, *c*) are then

$$\partial_t \boldsymbol{u} + (\boldsymbol{u} \cdot \nabla)\boldsymbol{u} = -\nabla p + \nabla^2 \boldsymbol{u} + \frac{Q}{\xi}(\nabla \wedge \boldsymbol{B}) \wedge \boldsymbol{B}, \tag{2.3a}$$

$$\partial_t \boldsymbol{B} = \frac{1}{\xi}\nabla^2 \boldsymbol{B} + \nabla \wedge (\boldsymbol{u} \wedge \boldsymbol{B}). \tag{2.3b}$$

A steady-state solution of the governing equations is circular-Couette flow, $\tilde{\boldsymbol{u}} = (0, \tilde{u}_\theta, 0)$ where $\tilde{u}_\theta = Ar + B/r$. The constants A and B are determined by the no-slip boundary conditions. We set $\boldsymbol{u} = \tilde{\boldsymbol{u}} + \boldsymbol{u}'$ and $p = \tilde{p} + p'$. The deviation, $\boldsymbol{u}'$, then satisfies the homogeneous Dirichlet boundary condition, $\boldsymbol{u}' = \boldsymbol{0}$ at R_1, R_2. Subtracting the Navier–Stokes equation for $\tilde{\boldsymbol{u}}$ from (2.3*a*), the evolution of $\boldsymbol{u}'$ is now described by

$$(\partial_t - \nabla^2)\boldsymbol{u}' = \boldsymbol{N} - \nabla p', \quad \nabla \cdot \boldsymbol{u}' = 0, \tag{2.4a,b}$$

$$\left(\partial_t - \frac{1}{\xi}\nabla^2\right)\boldsymbol{B} = \boldsymbol{N}_B, \quad \nabla \cdot \boldsymbol{B} = 0, \tag{2.4c,d}$$

with nonlinear terms,

$$\boldsymbol{N} = \frac{Q}{\xi}(\nabla \wedge \boldsymbol{B}) \wedge \boldsymbol{B} - (\boldsymbol{u} \cdot \nabla)\boldsymbol{u}' - (\boldsymbol{u}' \cdot \nabla)\tilde{\boldsymbol{u}}, \quad \boldsymbol{N}_B = \nabla \wedge (\boldsymbol{u} \wedge \boldsymbol{B}). \tag{2.4e,f}$$

The magnetic Prandtl number ξ is very small in liquid metals available in the laboratory, so we set $\boldsymbol{B} = \boldsymbol{B}_0 + \xi \boldsymbol{b}$. In the limit $\xi \to 0$ the governing equations become

$$(\partial_t - \nabla^2)\boldsymbol{u}' = \boldsymbol{N} - \nabla p', \quad \nabla \cdot \boldsymbol{u}' = 0, \tag{2.5a,b}$$

$$\nabla^2 \boldsymbol{b} = \boldsymbol{N}_B, \quad \nabla \cdot \boldsymbol{b} = 0, \tag{2.5c,d}$$

where

$$\boldsymbol{N} = Q(\nabla \wedge \boldsymbol{b}) \wedge \boldsymbol{B}_0 - (\boldsymbol{u} \cdot \nabla)\boldsymbol{u}' - (\boldsymbol{u}' \cdot \nabla)\tilde{\boldsymbol{u}}, \quad \boldsymbol{N}_B = -\nabla \wedge (\boldsymbol{u} \wedge \boldsymbol{B}_0). \tag{2.5e,f}$$

Note that these equations are descriptive rather than predictive for $\boldsymbol{b}$.

3. Boundary conditions

The governing equations (2.4) represent a tenth-order system in r and we therefore require ten boundary conditions. The first six are simply the no-slip condition, $u_r = u_\theta = u_z = 0$ applied at the boundaries $r = R_1$ and $r = R_2$. The boundary conditions for the magnetic field depend on the nature of the container, as discussed by Roberts (1964), who determined conditions for arbitrary values of electrical conductivity. The experiments by Donnelly & Ozima (1962) used mercury with Perspex and stainless-steel containers. Only a small difference was found between the results obtained using different containers. Hereafter we consider only the simple case of insulating boundaries.

Ampere's law states that $\boldsymbol{J} = \xi^{-1}\nabla \wedge \boldsymbol{B} = 0$, when $r < R_1$ or $r > R_2$, as the current within an insulator must be zero. It follows that the magnetic field is irrotational and can be expressed in terms of a potential, ψ, in the following way:

$$\boldsymbol{B} = -\nabla\psi, \quad -\nabla \cdot \boldsymbol{B} = \nabla^2 \psi = 0. \tag{3.1}$$

This equation can be solved for ψ by separation of variables, $\psi(r,\theta,z) = R(r)\,\Theta(\theta)\,Z(z)$. In our periodic coordinates we obtain,

$$\frac{\Theta''(\theta)}{\Theta(\theta)} = -m^2, \quad \frac{Z''(z)}{Z(z)} = -\alpha^2, \tag{3.2}$$

where m is integer. The equation for $R(r)$ satisfies the modified Bessel equation,

$$\frac{1}{r}R'(r) + R''(r) - \left(\alpha^2 + \frac{m^2}{r^2}\right)R(r) = 0. \tag{3.3}$$

The boundary conditions for $R(r)$ then depend on the type of solution.

If ψ is independent of θ and z ($m = \alpha = 0$) then ψ must be constant and so $\boldsymbol{B} = \boldsymbol{0}$. But this means that we have three conditions at each boundary, and we only need two. However, the divergence-free condition implies that a solution which is independent of θ and z must have no radial component. It is therefore sufficient to take

$$B_\theta = B_z = 0. \tag{3.4}$$

If ψ is independent of z but depends on θ ($\alpha = 0, m \neq 0$) then $R(r) = r^{\pm m}$. Recalling that $\boldsymbol{B} = \nabla\psi$, we have,

$$\partial_\theta B_r = \pm m B_\theta, \quad B_z = 0. \tag{3.5}$$

If ψ is z-dependent ($\alpha \neq 0$) then $R(r) = \mathscr{B}_m(r)$ where $\mathscr{B}_m(r)$ denotes either of the modified Bessel functions $I_m(\alpha r), K_m(\alpha r)$. We obtain

$$\partial_z B_r = \frac{\partial_r \mathscr{B}_m}{\mathscr{B}_m} B_z, \quad \frac{1}{r}\partial_\theta B_z = \partial_z B_\theta. \tag{3.6}$$

In the outer region $r > R_2$ the field tends to zero, $\boldsymbol{B} \to 0$ as $r \to \infty$, and in the inner region $r < R_1$ $\boldsymbol{B}$ must remain finite, which implies that we take

$$R(r) = \begin{cases} I_m(\alpha r) & r^{+m} & r \leqslant R_1 \\ \text{or} & \text{on} & \\ K_m(\alpha r) & r^{-m} & r \geqslant R_2 \end{cases} \tag{3.7}$$

The two relations (3.4) and (3.5) or (3.6) applied at the points $r = R_1$ and $r = R_2$, given the appropriate function from (3.7), are equivalent to Roberts' insulating boundary conditions. In this way we have the remaining four boundary conditions required.

4. Formulation and solution

The difficulty with primitive-variable formulations is how to ensure a divergence-free field. A possible solution is to combine time splitting and pressure projection. The divergence of the momentum equation gives a Poisson equation for the pressure which is used to project the velocity into the space of solenoidal functions. No pressure term occurs naturally in the induction equation, and if not removed divergence can build up in the solution for the magnetic field, especially at larger magnetic Prandtl numbers. However, an arbitrary projection function could be added in order for the divergence to scale with the timestep. Marcus (1984) used an influence matrix method in order to implement the correct boundary conditions for the pressure (Rempfer 2002). This technique leads to a divergence that is zero to machine accuracy. In both methods an adjustment to the field is made at each timestep. However, for the hydromagnetic case there is no timestep in the small Prandtl number limit; without potentials it is difficult to invert the Poisson equation for the magnetic field

whilst simultaneously ensuring it is divergence-free. We propose a formulation able to cope with both finite Prandtl numbers and the small Prandtl number limit without significant adjustments.

Popular in MHD is the toroidal–poloidal potentials form where variables are decomposed as $\boldsymbol{A} = \boldsymbol{\nabla} \wedge (\psi \boldsymbol{e}) + \boldsymbol{\nabla} \wedge \boldsymbol{\nabla} \wedge (\phi \boldsymbol{e})$ where $\boldsymbol{e}$ is a vector constant. To eliminate the pressure in the momentum equation it is common to take the e-components of the first and second curls as the governing equations for the velocity. For the magnetic field it is sufficient to take the e-components of the induction equation and its first curl.

In spherical geometry one assumes $\boldsymbol{e} = \boldsymbol{r}_s$, the spherical radius. Taking r_s-components of successive curls, the Navier–Stokes and induction equations separate into one equation for each of the potentials, Hollerbach (2000*b*). Unfortunately complications can arise if this method is used in cylindrical geometry. The choice $\boldsymbol{e} = \hat{\boldsymbol{z}}$ leads to separate equations for each of the potentials but raises the order of the equations in r. However, Marqués (1990) has derived the extra boundary conditions required for the hydrodynamic problem.

Taking the second curl leads to an operator acting on one of the potentials in the form of double Laplacians. In spherical geometry Tilgner & Busse (1997) successfully implemented a second-order code using this formulation with stress-free boundaries. Hollerbach (2000*b*) also used this formulation with no-slip boundary conditions but found it to be unstable, even for very small timesteps, unless an implicit first-order time discretization was used. In the cylindrical geometry Rüdiger & Feudel (2000) used the formulation of Marqués (1990), but similarly used a first-order method to avoid numerical difficulties. It is not at all clear that higher derivatives necessarily entail numerical instability in hydrodynamical solvers. However, for reasons that become apparent when the velocity field is discussed (§ 4.3), the second curl is avoided.

Instead we are motivated by a parallelism with the magnetic field and take only the first curl. As the pressure has not been eliminated, we also take the divergence of the momentum equation. A single-curl formulation was proposed by Glatzmaier (1984) in the spherical geometry and has proved very successful.

We have made the choice $\boldsymbol{e} = \boldsymbol{r}$ where $\boldsymbol{r}$ is the cylindrical-polar radius. This choice gives equations which couple the potentials, but this is no particular problem; with primitive variables r- and θ-components are coupled. Fortunately, although we still raise the order of the equations, the extra derivatives appear in the periodic coordinates and so no extra boundary conditions are required. To ensure capture of all possible solutions extra terms along $\hat{\boldsymbol{\theta}}$ and $\hat{\boldsymbol{z}}$ are added, in order to accommodate solutions that are independent of both θ and z. A full expansion of variables has the form

$$\boldsymbol{A} = \psi_0 \hat{\boldsymbol{\theta}} + \phi_0 \hat{\boldsymbol{z}} + \boldsymbol{\nabla} \wedge (\psi \boldsymbol{r}) + \boldsymbol{\nabla} \wedge \boldsymbol{\nabla} \wedge (\phi \boldsymbol{r}), \tag{4.1}$$

where $\psi(r, t, z)$, $\phi(r, t, z)$ and $\psi_0(r)$, $\phi_0(r)$ contain the periodic and non-periodic parts respectively. We discuss first the formulation for the magnetic field, as it motivates the method for the velocity.

4.1. *The magnetic field*

The magnetic field is expanded as

$$\boldsymbol{B} = \mathscr{T}_0 \hat{\boldsymbol{\theta}} + \mathscr{P}_0 \hat{\boldsymbol{z}} + \boldsymbol{\nabla} \wedge (\mathscr{T} \boldsymbol{r}) + \boldsymbol{\nabla} \wedge \boldsymbol{\nabla} \wedge (\mathscr{P} \boldsymbol{r}), \tag{4.2}$$

and substituted into the induction equation, (2.4*d*). For the non-periodic potentials $\mathscr{T}_0, \mathscr{P}_0$ the governing equations are obtained from the θ-, z-components,

$$\left(\partial_t - \frac{1}{\xi}\left(\nabla^2 - \frac{1}{r}\right)\right)\mathscr{T}_0 = \hat{\boldsymbol{\theta}} \cdot \boldsymbol{N}_B, \tag{4.3a}$$

$$\left(\partial_t - \frac{1}{\xi}\nabla^2\right)\mathscr{P}_0 = \hat{\boldsymbol{z}} \cdot \boldsymbol{N}_B. \tag{4.3b}$$

with boundary conditions at R_1, R_2,

$$\mathscr{T}_0 = 0, \quad \mathscr{P}_0 = 0. \tag{4.4}$$

The periodic potentials $\mathscr{T}, \mathscr{P}$ are assumed to be of form $\mathrm{e}^{\mathrm{i}(\alpha z + m\theta)}$. In order to match the boundary conditions a spectral expansion will be required. There is no pressure term to eliminate here, so we take the r-components of the induction equation and its first curl,

$$\frac{2}{\xi r^2}\partial_{\theta z}\mathscr{T} - \nabla_c^2\left(\partial_t - \frac{1}{\xi}\tilde{\nabla}^2\right)\mathscr{P} - \frac{2}{\xi r^3}\partial_{r\theta\theta}\mathscr{P} = \frac{1}{r^2}\boldsymbol{r} \cdot \boldsymbol{N}_B, \tag{4.5a}$$

$$-\nabla_c^2\left(\partial_t - \frac{1}{\xi}\tilde{\nabla}^2\right)\mathscr{T} - \frac{2}{\xi r^3}\partial_{r\theta\theta}\mathscr{T} + \frac{2}{r^2}\left(\partial_t - \frac{2}{\xi}\nabla^2\right)\partial_{\theta z}\mathscr{P} = \frac{1}{r^2}\boldsymbol{r} \cdot \nabla \wedge \boldsymbol{N}_B, \tag{4.5b}$$

where

$$\tilde{\nabla}^2 = \nabla^2 + \frac{2}{r}\partial_r, \quad \nabla_c^2 = \frac{1}{r^2}\partial_{\theta\theta} + \partial_{zz}, \tag{4.6}$$

with boundary conditions at R_1, R_2,

$$\alpha = 0: \qquad \partial_\theta \mathscr{T} = 0, \quad \left(\nabla_c^2 \pm \frac{m}{r}\partial_r\right)\partial_\theta \mathscr{P} = 0; \tag{4.7a}$$

$$\left.\begin{aligned} &\nabla_c^2 \mathscr{T} - \frac{2}{r^2}\partial_{\theta z}\mathscr{P} = 0, \\ &\frac{1}{r}\partial_\theta \mathscr{T} - \left(\frac{\mathscr{B}_m}{\partial_r \mathscr{B}_m}\nabla_c^2 + \frac{2}{r} + \partial_r\right)\partial_z \mathscr{P} = 0. \end{aligned}\right\} \tag{4.7b}$$

$$\alpha \neq 0:$$

This formulation is suitable for the small Prandtl number limit (2.5), relevant to laboratory liquid metals. We expand $\boldsymbol{b}$ by the same potentials and make the replacements

$$\partial_t \to 0, \quad -\frac{1}{\xi} \to 1,$$

throughout. The field $\boldsymbol{b}$ satisfies the same boundary conditions as $\boldsymbol{B}$.

Having settled on a formulation of the equations, we now discuss the numerical method.

4.2. *Numerical method*

It is customary to adjust the radial range into the unit interval, so a new radial variable x is defined as

$$r = R_1 + x, \quad R_1 = \eta/(1-\eta), \quad x \in [0, 1]. \tag{4.8}$$

If a field is expected to have m_1-fold rotational symmetry, such as the case of wavy modes, then variables are expanded as

$$A(x,\theta,z,t)=\sum_{n=0}^{N}\sum_{|k|<K}\sum_{|m|<M}A_{nkm}(t)T_n^*(x)\,\mathrm{e}^{\mathrm{i}(\alpha kz+m_1m\theta)} \tag{4.9}$$

on the domain $[0,1]\times[0,2\pi/m_1]\times[0,2\pi/\alpha]$ where $T_n^*(x)$ is the nth shifted Chebyshev polynomial. Variables are collocated on the $N+1$ extrema of $T_N(x)$. This arrangement of points is well suited to our problem with the points concentrated near the boundaries.

As the velocity and magnetic field are coupled by the nonlinear terms it makes sense to treat them explicitly. Nonlinear terms are evaluated pseudospectrally, where necessary. Large terms in the zero modes, like circular-Couette flow and the imposed magnetic field, can be extracted and calculated exactly. Let q indicate the time discretization $t_q=q\Delta t$ with $q=0,1,2,\ldots$. We choose to use second-order Adams–Bashforth to estimate $\boldsymbol{N}_B$ at the intermediate time $q+\frac{1}{2}$.

The linear terms are easier to evaluate and are timestepped using the implicit Crank–Nicolson method. Substituting the spectral expansion in the governing equations (4.5) and the boundary conditions (4.7), after collocation the problem for each k,m mode becomes

$$\boldsymbol{X}\begin{bmatrix}\mathscr{T}\\ \mathscr{P}\end{bmatrix}^{q+1}=\boldsymbol{Y}\begin{bmatrix}\mathscr{T}\\ \mathscr{P}\end{bmatrix}^{q}+\begin{bmatrix}N_1\\ N_2\end{bmatrix}^{q+1/2}, \tag{4.10}$$

where $\boldsymbol{X}$ and $\boldsymbol{Y}$ are matrices. The vector $[\mathscr{T},\mathscr{P}]^q$ contains the spectral coefficients of the potentials at time t_q. The nonlinear terms have been evaluated on the collocation points. Despite the Fourier expansions, the matrices $\boldsymbol{X},\boldsymbol{Y}$ are real and are calculated by the same routine, as they differ only by a scalar constant, namely $\pm\Delta t$.

With this formulation modifications for the small Prandtl number limit (2.5) are relatively minor. The magnetic field is now completely defined by the velocity at some particular time t_q, For each k,m mode the problem in matrix-vector form is now simply

$$\boldsymbol{X}\begin{bmatrix}\mathscr{T}\\ \mathscr{P}\end{bmatrix}^{q}=\begin{bmatrix}N_1\\ N_2\end{bmatrix}^{q}. \tag{4.11}$$

The matrices $\boldsymbol{X}$ are calculated by the same routines as above as, again, they only differ by scalar constants.

4.3. *The velocity field*

Unless there is an externally imposed velocity field, there is no non-periodic pressure to be eliminated. The non-periodic part of the velocity is then treated in the same manner as the magnetic field, i.e.

$$\left(\partial_t-\left(\nabla^2-\frac{1}{r}\right)\right)\psi_0=\hat{\boldsymbol{\theta}}\cdot\boldsymbol{N}, \tag{4.12a}$$

$$(\partial_t-\nabla^2)\phi_0=\hat{\boldsymbol{z}}\cdot\boldsymbol{N}, \tag{4.12b}$$

with boundary conditions

$$\psi_0=\phi_0=0 \tag{4.13}$$

on R_1,R_2.

For the periodic part we follow the procedure applied to the magnetic field and take only the first curl. As the pressure has not been eliminated, we also take the divergence of the momentum equation. The equations obtained are

$$\frac{2}{r^2}\partial_{\theta z}\psi - \nabla_c^2(\partial_t - \tilde{\nabla}^2)\phi - \frac{2}{r^3}\partial_{r\theta\theta}\phi = \frac{1}{r^2}\boldsymbol{r}\cdot(\boldsymbol{N} - \nabla p), \tag{4.14a}$$

$$-\nabla_c^2(\partial_t - \tilde{\nabla}^2)\psi - \frac{2}{r^3}\partial_{r\theta\theta}\psi + \frac{2}{r^2}(\partial_t - 2\nabla^2)\partial_{\theta z}\phi = \frac{1}{r^2}\boldsymbol{r}\cdot\nabla\wedge\boldsymbol{N}, \tag{4.14b}$$

$$\nabla^2 p = \nabla\cdot\boldsymbol{N}. \tag{4.14c}$$

These equations may look complicated enough, but taking the second curl they are much worse! However, they simplify considerably for the axisymmetric problem. Note also the simplification that the linear differential operators on the left-hand sides of (4.5*a*, *b*) and (4.14*a*, *b*) are the same with $\xi \to 1$. Fourth-order derivatives have been avoided, otherwise as $|\mathrm{d}^p T_n^*(x)/\mathrm{d}x^p| = O(n^{2p})$ matrices can become difficult to invert accurately with larger truncations.

Every governing equation is only second order in r, and therefore all equations have the same number of associated boundary conditions. This permits us to take the same radial truncation N for all variables, so all matrices are likewise of the same size. This simplifies the actual implementation enormously. In fact, we timestep the governing equations (4.14*a*, *b*), the same way as the magnetic field,

$$\boldsymbol{X}\begin{bmatrix}\psi\\ \phi\end{bmatrix}^{*} = \boldsymbol{Y}\begin{bmatrix}\psi\\ \phi\end{bmatrix}^{q} + \begin{bmatrix}N_1\\ N_2\end{bmatrix}^{q+1/2}, \tag{4.15}$$

and the matrices $\boldsymbol{X}^{-1}, \boldsymbol{X}^{-1}\boldsymbol{Y}$ may be precomputed by the routine for the magnetic field as the equations are the same, but for scalar constants. Thus, linear terms for the velocity are also timestepped using Crank–Nicolson. Using this method, Marcus (1984) found that a numerical neutrally stable oscillation can occur at large wavenumbers. Fortunately this does not present a problem here, as the presence of the magnetic field tends to reduce the natural wavenumber.

Together, the evolution equations (4.14*a*, *b*) are only fourth order in r for the potentials, but there are six boundary conditions for the velocity. They are timestepped with boundary conditions $u_\theta = u_z = 0$, or

$$r\partial_z\psi + \partial_{r\theta}\phi = 0, \quad -\partial_\theta\psi + (2 + r\partial_r)\,\partial_z\phi = 0. \tag{4.16a,b}$$

The pressure-Poisson equation (4.14*c*) is inverted with the boundary condition $u_r = 0$, or

$$-r\nabla_c^2\phi = 0, \tag{4.16c}$$

essentially the no-penetration condition.

Inversion of (4.14*c*) requires a boundary condition, indirectly determined by (4.16*c*), in terms of p. The adjustment for pressure is

$$\begin{bmatrix}\psi\\ \phi\end{bmatrix}^{q+1} = \begin{bmatrix}\psi\\ \phi\end{bmatrix}^{*} - \boldsymbol{X}^{-1}\begin{bmatrix}\frac{1}{r}\partial_r p\\ 0\end{bmatrix}. \tag{4.17}$$

In order to separate ϕ^{q+1} from ψ^{q+1} we must work with $\boldsymbol{X}^{-1}$ rather than $\boldsymbol{X}$. For each k, m mode ∇_c^2 is just a scalar. Imposing $-r\nabla_c^2\phi^{q+1} = 0$ the boundary condition

Δt	% error in σ	% error in σ_B
0.01	5.74×10^{-2}	—
0.003	5.18×10^{-3}	1.48×10^{-2}
0.001	5.76×10^{-4}	1.65×10^{-3}
0.0003	5.2×10^{-5}	1.5×10^{-4}
0.0001	6×10^{-6}	2×10^{-5}

TABLE 1. Error in growth and decay rates. $N \to \infty$. For $\eta = 1/1.444$, $\alpha = 3.13$, $Re_1 = 80$, $Re_2 = 0$ the growth rate is $\sigma = 0.430108693$ (Barenghi 1991). For the magnetic field $m = 1$, $\sigma_B \xi = 14.055585$, $\xi = 1$. The error is proportional to Δt^2.

Q	α_c	N	Re_c
30	2.69	8	280.97
		10	281.05
100	1.73	8	463.20
		10	463.52
300	0.928	8	796.52
		10	798.57
		12	798.55

TABLE 2. Critical Reynolds numbers for varying numbers of modes and magnetic field strengths; $\eta = 0.95$ with insulating walls. For the largest number of modes in each case the values are the same to five significant figures as the results of Roberts' (1964) calculations.

becomes

$$\hat{\boldsymbol{X}}^{-1} \left(\frac{1}{r} \partial_r p \right) = \phi^*, \tag{4.18}$$

where $\hat{\boldsymbol{X}}^{-1}$ is the lower left quadrant of $\boldsymbol{X}^{-1}$. Condition (4.18) is implemented in the usual manner by multiplying on the left with the coefficients $T_n^*(x)$ at the boundaries.

5. Results

5.1. *Linear stability*

The linear part of the code is shared between the velocity and magnetic fields. Appropriate tests are determining the critical Reynolds number, Re_c, for the onset of Taylor-vortex flow in the presence/absence of a magnetic field, and determining the growth/decay rates of either field.

An eigenfunction of the linearized equations grows or decays exponentially at a rate σ. Barenghi (1991) examined convergence with Δt for the velocity by comparing with a known growth rate. A simple initial disturbance to the appropriate mode is $\phi \propto x^2(1-x)^2 \sin \alpha z$, or equivalently $\phi_{0,\pm1,0} = 3\Delta$, $\phi_{2,\pm1,0} = -4\Delta$, $\phi_{4,\pm1,0} = \Delta$, which satisfies the boundary conditions and mimics TVF surprisingly well.

To ensure that the boundary conditions for the magnetic field have been set up correctly we check our method against analytically derived decay rates (see the Appendix). Table 1 shows results of the test of growth rates and the comparison with Barenghi (1991). Note that the error is proportional to Δt^2.

To check the interaction of the two fields and the case $\xi \to 0$ we compare the onset of TVF with Roberts (1964). Table 2 shows the number of modes required to reproduce a few of Roberts' results to five significant figures.

N	K	u_r		
		$Re_1 = 72.4569$	106.066	150.0
10	6	4.236577	17.94932	33.48869
	8	4.236615	17.97669	33.66495
	12	4.236616	17.97902	33.70222
16	6	4.233596	17.94086	33.45839
	8	4.233635	17.96816	33.64135
	12	4.233635	17.97046	33.67982
—	—	4.23363	17.9705	33.6805

TABLE 3. Radial velocity at the outflow. $\Delta t \to 0$; $\eta = 0.5$, $x = 0.5$, $\alpha = 3.1631$, and a fixed outer cylinder. In the last row are the values for $Re_1 = 72.4569$, 106.066, 150.000 (Jones 1985).

Re_1/Re_c	$2\pi/\alpha$	Marcus	Measured
3.98	2.40	0.3443 ± 0.0001	0.3440 ± 0.0008
3.98	3.00	0.3344 ± 0.0001	0.3347 ± 0.0007
5.97	2.20	0.3370 ± 0.0001	0.3370 ± 0.0002

TABLE 4. Wave speeds expressed as a fraction of the angular velocity of the inner cylinder. $\eta = 0.868$, $Re_c = 115.1$, $m_1 = 6$.

5.2. *Nonlinear two-dimensional flow*

The saturation to a steady flow, for some not too large $Re_1 > Re_c$, provides a testing ground for the evaluation of nonlinear terms. Barenghi (1991) compares values for velocities at the outflow which are in agreement with results obtained by Jones (1985) using a different method. In table 3 we examine convergence with N, K. Generally we find that convergence is quicker in z than r, and for a given truncation accuracy decreases with increasing Re_1. More energy is found in the higher modes as Re_1 is increased.

5.3. *Wave speeds in wavy TVF*

A simple small wavy perturbation to axisymmetric TVF that satifies the boundary conditions is $\psi \propto x^2(1-x)^2 \sin m_1\theta$ for some wavy mode m_1. The perturbation will either decay or grow and saturate depending on whether or not the parameters are in the wavy TVF regime. King *et al.* (1984) compared wave speeds founds from physical experiments with numerical calculations. They found that "the wavespeed is a sensitive indicator of the accuracy of a numerical code"... "any compromise in numerical resolution changes the wavespeed by several percent". They also argue that the wave speed can be measured more precisely, both in experiment and numerically, than torques which are dependent on axial wavelength (see the comparison with torque experiments in § 6).

A few of the results used by Marcus (1984) as a test for his numerical method are given in table 4. Marcus' numerical results were well within the range of experimental error of about 1%. Calculations with our code gave results all within 0.1% of Marcus' values.

6. Nonlinear hydromagnetic flow and comparison with experiment

It should first be noted that the results of the previous section agree well with experiments. In this section we directly compare our results with hydromagnetic torque experiments.

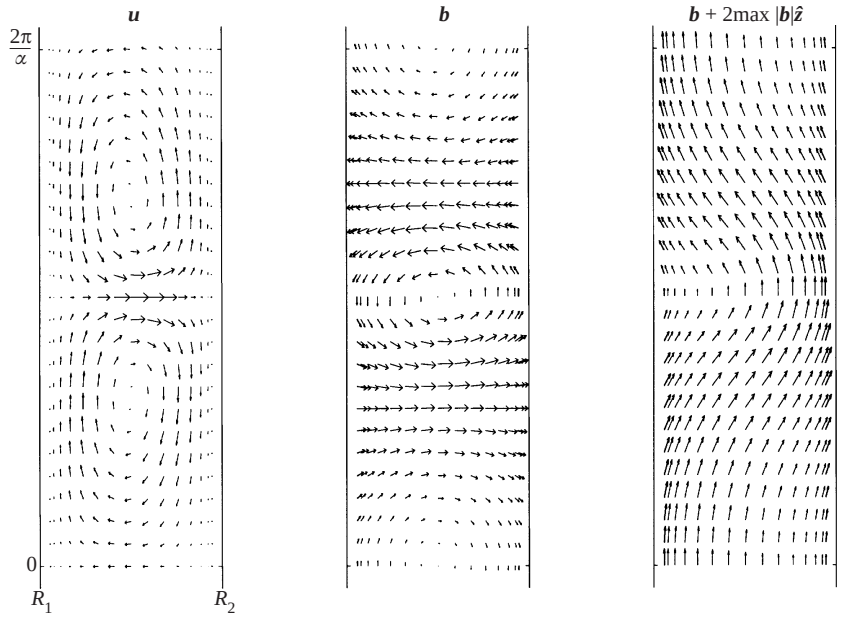

FIGURE 1. Hydromagnetic flow in the presence of an imposed axial field. $Q = 180$, $Re_1 = 1.5Re_c$, $Re_c = 619$, $\eta = 0.95$, $\alpha = 1.24$. The right-most plot demonstrates that the field lines are dragged by the in- and outflows.

The torque per unit axial length on the inner cylinder is defined as

$$G = \frac{\alpha r}{2\pi}\int_0^{2\pi} r\,\mathrm{d}\theta \int_0^{2\pi/\alpha} \mathrm{d}z \left(\frac{1}{r} - \partial_r\right) u_\theta \bigg|_{r=R_1}. \tag{6.1}$$

There is no magnetic torque with insulating boundaries. For an axisymmetric flow and given the expansion for the velocity (4.1), this simplifies to

$$G = 2\pi r^2 \left(\frac{1}{r} - \partial_r\right)(\psi_0 + \tilde{u}_\theta)\bigg|_{r=R_1}. \tag{6.2}$$

The ratio of the effective viscosity of the flow to the kinematic viscosity of the fluid is $G/\tilde{G}$ where $\tilde{G}$ is the component of the torque due only to the underlying circular-Couette flow, $\tilde{u}_\theta$.

Typical nonlinear steady fields in the presence of an imposed axial field are shown in figure 1. The main difference between the hydrodynamic and the hydromagnetic cases is the axial elongation of the Taylor cells. Not much difference is evident between the eigenfunctions and the saturated fields other than that the vortex centres move slightly outwards and closer together towards the outflow.

Figure 2 shows experimental results obtained by Donnelley & Ozima (1962) with mercury and Perspex cylinders. Also shown are torques for axisymmetric calculations with their aspect ratio, $\eta = 0.95$, and results of an amplitude expansion calculated by Tabeling (1981) in the narrow gap limit.

As the Reynolds number is increased there is good agreement between our numerical method, Tabeling's amplitude expansion and Donnelly's experiment, until Donnelly's results deviate from both ours and Tabeling's calculations. The points

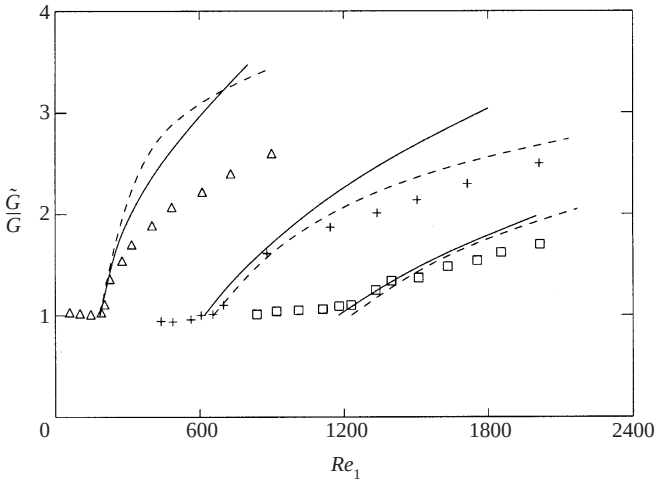

FIGURE 2. Comparison of torques. Experimental results with $\eta = 0.95$. $\triangle$, $Q = 0$; $+$, $Q = 180$; $\square$, $Q = 652$. Solid line, our numerical results. Dashed line, Tabeling's expansion about the Reynolds number in the narrow gap limit.

plotted in figure 2 are time averages as significant fluctuations were observed. Tabeling conjectured that this is due to the appearance of wavy modes. With $Q = 0$ the onset of wavy modes is not far above the onset of TVF and in simulations of these modes we find a reduced torque.

Note that if an axial magnetic field is imposed the onset of wavy modes is significantly inhibited. A detailed investigation of the linear and nonlinear aspects of the wavy modes will be presented in the next paper of this series. Here it suffices to note the good agreement between our calculations and the experiment in the weakly nonlinear axisymmetric regime.

7. Discussion

In conclusion, we have developed a formulation of the governing MHD equations of the cylindrical Couette geometry, suitable for timestepping in the nonlinear regime. Results agree well with experiments.

Although the equations do not decouple in the linear part, and we must treat mean flows separately, the formulation is similar to that used by Galtzmaier (1984) in spherical geometry. We use potentials for the velocity yet do not eliminate the pressure. This has several advantages. Our motivation for adopting such a formulation is that the magnetic field then shares the same formulation as the velocity, dramatically reducing the potential for error. Only a relatively small part of our code is dedicated entirely to the magnetic field; this feature is important for testing, as there are fewer results with which to compare our results. Furthermore, it can also accommodate the small Prandtl number limit with only minor adjustments. The choice of governing equations which are only second order in r makes the method accurate and matrices easily invertible. This feature also enables us to take the same radial truncation for all variables, if we desire, simplifying implementation a great deal.

We have opted to use potentials which ensure divergence-free fields. Primative variable formulations for time integration of the Navier–Stokes equations, such as Marcus (1984) and Quartapelle & Verri (1995) in this geometry, do not in general

extend naturally to the magnetic field. In particular, they are not well suited to the small Prandtl number limit, relevant to liquid metals available in the laboratory.

For the axisymmetric case the expansion by potentials is essentially the same as that used by Barenghi (1991) and Jones (1985) and results appear to be very similar in terms of accuracy. Although we have one extra equation, the actual form of our equations is simpler because we avoided taking the second curl.

Our method is second order in time and exhibits good temporal stability, We have not encountered the difficulties experienced by Hollerbach (2000*b*) and Rüdiger & Feudel (2000) with three-dimensional potential formulations and no-slip boundaries. Using the implict Euler method on the linear terms reduces the method to $O(\Delta t/Re, \Delta t^2)$. With finite magnetic Prandtl numbers the magneto-rotational instability (Rüdiger & Zhang 2001; Willis & Barenghi 2002) leads to Reynolds numbers which can be surprisingly low and the $O(\Delta t/Re)$ error would dominate.

Results obtained using our method compare well with existing hydrodynamic literature with respect to the nonlinear equilibration of Taylor-vortex flow (Barenghi 1991), the onset of wavy modes (Jones 1985) and the wave speed of wavy modes (Marcus 1984). In the presence of a magnetic field the results also compare well for the linear stability of circular-Couette flow (Roberts 1964), and in the nonlinear range the amplitude expansion of Tabeling (1981) and experiments of Donnelly & Ozima (1962).

In further work, we will use this method to analyse nonlinear three-dimensional hydromagnetic Taylor–Couette flow.

The authors wish to thank Anvar Shukurov and Wolfgang Dobler for stimulating discussions and encouragement during this work, and to a referee for helpful clarifications.

Appendix. Decay of the magnetic field

To derive the decay rate of the magnetic field when $\boldsymbol{u} = \boldsymbol{0}$ we use a mixture of analytical and numerical methods, different from the numerical technique used to solve the MHD equations. We express the magnetic field in terms of two scalar potentials,

$$\boldsymbol{B} = \nabla \wedge (\mathscr{T}\hat{\boldsymbol{z}}) + \nabla \wedge \nabla \wedge (\mathscr{P}\hat{\boldsymbol{z}}). \tag{A 1}$$

Each of $\mathscr{T}$, $\mathscr{P}$ is expanded and we seek eigensolutions for the magnetic field of the form

$$A(r,\theta,z) = \sum_{k,m=-\infty}^{\infty} A_{km}(r)\,\mathrm{e}^{-\sigma t+\mathrm{i}(\alpha k z+m\theta)}, \tag{A 2}$$

where σ is the decay rate. Substitution into (2.3*c*) yields the Bessel equation,

$$\frac{1}{r}\partial_r A_{km}(r) + \partial_{rr} A_{km}(r) + \left(\hat{\sigma}^2 - \frac{m^2}{r^2}\right) A_{km}(r) = 0, \quad \hat{\sigma}^2 = \sigma\xi - \alpha^2 k^2, \tag{A 3}$$

which has solution

$$A_{km}(r) = A^J_{km} J_m(\hat{\sigma} r) + A^Y_{km} Y_m(\hat{\sigma} r). \tag{A 4}$$

Matching at the two boundaries the conditions (3.6)–(3.8) for the magnetic field defines the problem

$$\boldsymbol{M}(\hat{\sigma})[\mathscr{T}^J_{km}, \mathscr{T}^Y_{km}, \mathscr{P}^J_{km}, \mathscr{P}^Y_{km}]^T = \boldsymbol{0}, \tag{A 5}$$

k		$\sigma\xi$			
		$m=0$	1	2	3
0	($\mathscr{T}$)	10.634504	2.525434*	6.259403	11.170948
	($\mathscr{P}$)	9.613411	10.634504	13.640533	18.474045
1	(1st)	14.919861	14.760834	16.619549	
	(2nd)	20.431404	22.010271	25.611050	
2	(1st)	45.851458	45.868780		
	(2nd)	49.822104	51.678920		

TABLE 5. Decay of the magnetic field, $\sigma\xi$, for $\eta = 0.35$, $\alpha = 3.13$. When $k = 0$ toroidal and poloidal modes separate and their slowest decaying modes are given; α is a redundant parameter in this case. Otherwise they couple and the first two modes are given. The dominant mode is marked *.

for the four unknown coefficients. The quantity $\boldsymbol{M}$ is a 4×4 matrix and is real if $\hat{\sigma}$ is real (non-oscillatory decay modes). The slowest decaying eigensolution for $\boldsymbol{B}$ is determined by the smallest $\hat{\sigma}$ such that $\det \boldsymbol{M}(\hat{\sigma}) = 0$. Results are shown in table 5.

REFERENCES

BARENGHI, C. F. 1991 Computations of transitions and Taylor vortices in temporally modulated Taylor–Couette flow. *J. Comput. Phys.* **95**, 175–194.

BAYLIS, J. A. & HUNT, J. C. R. 1971 MHD flow in an annular channel; theory and experiment. *J. Fluid Mech.* **48**, 423–428.

CHANDRASEKHAR, S. 1961 *Hydrodynamic and Hydromagnetic Stability*. Clarendon.

CHANG, T. S. & SARTORY, W. K. 1967 On the onset of instability by oscillatory modes in hydrodynamic Couette flow. *Proc. R. Soc. Lond.* A **301**, 451–471.

DAVEY, A. 1962 The growth of Taylor vortices in flow between rotating cylinders. *J. Fluid. Mech.* **14**, 336–368.

DONNELLY, R. J. & CALDWELL, D. R. 1963 Experiments on the stability of hydromagnetic Couette flow. *J. Fluid Mech.* **19**, 257–263.

DONNELLY, R. J. & OZIMA, M. 1962 Experiments on the stability of flow between rotating cylinders in the presence of a magnetic field. *Proc. R. Soc. Lond.* A **226**, 272–286.

GAILITIS, A., LIELAUSIS, O., PLATACIS, E., DEMENT'EV, S., CIFERSONS, A., GERBETH, G., GUNDRUM, T., STEFANI, F., CHRISTEN, M. & GOTTHARD, W. 2001 Magnetic field saturation in the Riga dynamo experiment. *Phys. Rev. Lett.* **86**, 3024–3027.

GLATZMAIER, G. A. 1984 Numerical simulations of stellar convective dynamos. 1. The model and method. *J. Comput. Phys.* **55**, 461–484.

HOLLERBACH, R. 2000*a* Magnetohydrodynamic flows in spherical shells. In *Physics of Rotating Fluids*, pp. 295–316. Springer.

HOLLERBACH, R. 2000*b* A spectral solution of the magneto-convection equations in sperical geometry. *Intl J. Numer. Meth. Fluids* **32**, 773–797.

JONES, C. A. 1985 Numerical methods for the transition to wavy Taylor vortices. *J. Comput. Phys.* **61**, 321–344.

KIKURA, H., TAKEDA, Y. & DURST, F. 1999 Velocity profile measurement of the Taylor vortex flow of a magnetic fluid using the ultrasonic Doppler method. *Exps. Fluids*, **26**, 208–214.

KING, G. P., LI, Y., LEE, W., SWINNEY, H. L. & MARCUS, P. S. 1984 Wave speeds in wavy Taylor-vortex Flow. *J. Fluid Mech.* **141**, 365–390.

KURZWEG, U. H. 1963 The stability of Couette flow in the presence of an axial magnetic field. *J. Fluid Mech.* **17**, 52–60.

LAURE, P., CHOSSAT, P. & DAVIAUD, F. 2000 Generation of magnetic field in the Couette–Taylor system. In *Dynamo and Dynamics, a Mathematical Challenge*, Nato science series II, vol. 26, pp. 17–24.

MARCUS, P. S. 1984 Simulation of Taylor–Couette flow. Part 1. Numerical methods and comparison with experiment. *J. Fluid Mech.* **146**, 45–64.

MARQUÉS, F. 1990 On boundary conditions for velocity potentials in confined flow. *Phys. Fluids* A **2**, 729–737.

NAGATA, M. 1996 Nonlinear solutions of modified plane Couette flow in the presence of a transverse magnetic field. *J. Fluid. Mech.* **307**, 231–243.

QUARTAPELLE, L. & VERRI, M. 1995 On the spectral solution of the three-dimensional Navier–Stokes equations in spherial and cylindrical regions. *Comput. Phys. Commun.* **90**, 1–43.

REMPFER, D. 2002 On boundary conditions for incompressible Navier–Stokes problems. Submitted to *J. Comput. Phys.*

ROBERTS, P. H. 1964 The stability of hydromagnetic Couette flow. *Proc. Camb. Phil. Soc.* **60**, 635–651.

RÜDIGER, G. & ZHANG, Y. 2001 MHD instability in differentially-rotating cylindric flows. *Astron. Astrophys.* **378**, 302–308.

RÜDIGER, S. & FEUDEL, F. 2000 Pattern formation in Rayleigh–Bénard convection in a cylindrical container. *Phys. Rev.* E **62**, 4927–4931.

STEIGLITZ, R. & MÜLLER, U. 2001 Experimental demonstration of a homogeneous two-scale dynamo. *Phys. Fluids* **13**, 561–564.

TABELING, P. 1981 Magnetohydrodynamic Taylor vortex flows. *J. Fluid Mech.* **112**, 329–345.

TAYLOR, G. I. 1923 Stability of a viscous liquid contained between two rotating cylinders. *Phil. Trans. R. Soc. Lond.* A **223**, 289–343.

TILGNER, A. & BUSSE, F. H. 1997 Finite-amplitude convection in rotating spherical fluid shells. *J. Fluid Mech.* **332**, 359–376.

VELIKHOV, E. P. 1959 Stability of an ideally conducting liquid flowing between cylinders rotating in a magnetic field. *J. Expl Theoret. Phys.* (*USSR*) **36**, 1398–1404.

WILLIS, A. P. & BARENGHI, C. F. 2002 Magnetic instability in a sheared azimuthal flow. *Astron. Astrophys.* (to appear).